Memory Window and Variability Modeling of Multi-Domain Al:HfO_2 Ferroelectric NAND Memory

Kuan-Hung Liu
Synopsys Taiwan
HsinChu, Taiwan
Kuan-Hung.Liu@synopsys.com

Tue Gunst
Synopsys Denmark
Copenhagen, Denmark
Tue.Gunst@synopsys.com

Ko-Hsin Lee
Synopsys Taiwan
HsinChu, Taiwan
Helen.Lee@synopsys.com

Anders Blom
Synopsys Inc.
Sunnyvale, CA, US
Anders.Blom@synopsys.com

Xi-Wei Lin
Synopsys Inc.
Sunnyvale, CA, US
Xi-Wei.Lin@synopsys.com

2024 International Conference on Simulation of Semiconductor Processes and Devices (SISPAD) | 979-8-3315-1635-2/24/$31.00 ©2024 IEEE | DOI: 10.1109/SISPAD62626.2024.10732967

***Abstract*—This paper presents simulation of a three-dimensional ferroelectric NAND memory using a multi-domain Ginzburg–Landau–Khalatnikov polarization model. The model parameters with a variation range following a Gaussian function are calibrated based on experimental polarization-electric field hysteresis for undoped and 5 mol% Al-doped HfO_2 thin films. The allowed memory window between program and erase states can be enlarged from 2.9 to 12.6V through the incorporation of Al dopant in HfO_2. The 3-sigma standard variation of threshold voltage change due to the grain-to-grain variability is also examined and estimated to be 0.57V. This polarization enhancement by substituting Hf with Al atom is also justified through atomistic simulation.**

Keywords—Ferroelectric, HfO_2, Al composition, Fe-NAND, Density functional theory, TCAD simulation

I. Introduction

3D NAND flash memory is a key driver of the massive data storage market and has the potential to enable the in-memory computing architecture. The data stored through trapping charges in a charge trap nitride (CTN) layer is widely adopted in current 3D NAND designs and the memory capacity is increased mainly by stacking more memory cells. Nevertheless, in the CTN-based architecture, vertical scaling is challenging due to the carrier migration induced cell-to-cell interference and high voltage operation, which poses a limitation on the spacer oxide thickness between two wordlines. Alternatively, 3D ferroelectric NAND (Fe-NAND) can be a candidate to improve the cell density. The polarity in ferroelectric cell can be maintained at small scale of few nanometers [1] and the operating voltage to alter the program and erase states is relatively lower compared to CTN-NAND [2]. Lately, the quad-level cell (QLC) operation has been demonstrated as well in 3D Fe-NAND with a memory window (MW) up to 10.5V and a minimum gap margin of 0.24V [2].

Among diverse ferroelectric thin films with perovskite structure, hafnia (HfO_2)-based fluorite ferroelectrics are more attractive to realize 3D Fe-NAND [2-3] thanks to its superior ferroelectricity at an ultra-thin thickness, relatively large coercive electric field and process compatibility with CMOS technology [4-5]. The ferroelectricity associated with the orthorhombic phase (o-phase) in HfO_2 material can be obtained under various process conditions and element doping is one promising way to controllably produce oxygen vacancies leading to an enhanced ferroelectricity [6]. It has been presented that the remnant polarization (P_r) values exhibiting 24 - 32.5 $\mu C/cm^2$ can be obtained for about 10nm-thick HfO_2 thin films doped with Si, Y, and Zr [7]. Apart from the doping elements mentioned above, Al is also a preferable dopant for ferroelectric HfO_2 thin films, since in the atomic layer deposition (ALD) the process temperature for Al_2O_3 is similar to HfO_2, which avoids the deterioration of surface roughness. In addition, the p-type doping benefits generation of donor-type oxygen vacancy defects. The ferroelectricity in Al:HfO_2 can depend on diverse factors, such as thin film thickness, film deposition process, Al composition, and thermal annealing treatment. A record remnant polarization as high as 50 $\mu C/cm^2$ has been reported in 10nm-thick 6.4 mol% Al-doped HfO_2 thin films in combination with a fast thermal quenching process [8].

In this paper, we first simulate the ferroelectricity change with Al doping in HfO_2 bulk in atomistic scale to inspect how the polarization can be enhanced with presence of Al. Since a HfO_2-based ferroelectric thin film fabricated by ALD is generally polycrystalline, the remnant polarization and the coercive field characteristics have grain-to-grain variations. Therefore, multi-domain ferroelectric simulation is considered based on the Ginzburg–Landau–Khalatnikov (GLK) polarization model. We then calibrate the GLK model parameters with respect to experimental values of remnant polarization and coercive field for undoped and 5 mol% Al doped HfO_2 thin films grown on Si substrate using ALD [6]. The extracted polarization model parameters are adopted for Fe-NAND simulations to examine the characteristics of memory window and grain-to-grain variability. It is found that the Fe-NAND with Al:HfO_2 thin film shows an enlarged MW compared to HfO_2, which thus has the potential for QLC operation.

II. Simulation Setup

A. Atomic Simulation for Al:HfO_2 Bulk

The correlation between atomic structure and ferroelectric characteristics of the single-domain polar orthorhombic Al:HfO_2 is investigated with Al content ranging from 0 to 10 mol%. The electronic structure of Al:HfO_2 is calculated using QuantumATK-DFT [9]. The atomic simulation is performed with PBEsol for exchange-correlation and with the PseudoDojo-Medium pseudopotential and localized basis set. The K-point sampling used a density of 12 Ang and a density mesh cutoff of 125 Hartree. The structure is relaxed until all forces are below 0.005 eV/Å, while constraining the space group symmetry. To calculate the remnant polarization, the Berry phase approach is applied. The doping by Al at Hf substitutional sites is modeled through virtual crystal

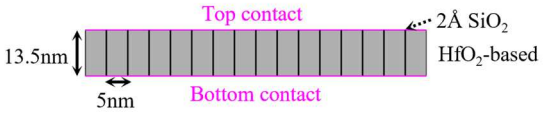

Fig. 1. Schematic of MFM capacitor with 13.5 nm-thick FE HfO_2 thin film divided into 16 regions with a grain size length of 5 nm.

approximation. Additionally, the energy barrier for polarization switching is calculated by the nudged elastic band (NEB) approach.

B. *TCAD Simulation for MFM Capacitor with Al:HfO_2 Thin Films*

For ferroelectric materials, the GLK equation describes ferroelectric properties in terms of free energy expanded as a power series in ferroelectric polarization and is represented as

$$F = \int_\Omega \alpha_i P_i^2 + \beta_i P_i^4 + \gamma_i P_i^6 + g_{ij}\left(\frac{\partial P_i}{\partial x_j}\right)^2 - E_i P_i + \frac{\varepsilon_0 \varepsilon_r}{2} E_i E_j d\Omega \quad (1)$$

where F is the free energy, P_i is the ferroelectric polarization component of the Cartesian coordinates (i, j=x, y, z), α_i, β_i, γ_i are the Landau coefficients, g_{ij} is the coefficient of polarization gradient, and E_i is the electric field component.

The parameter calibration for GLK polarization model is realized on a metal-ferroelectric-metal (MFM) capacitor structure with a thickness of 13.5 nm Al:HfO_2 thin film, as shown schematically in Fig. 1. The multi-domain behavior of ferroelectric layer is implemented in Synopsys' Sentaurus Device simulation tool [10] by separating the HfO_2-based layer into 16 regions of 5nm-long grain size, separated by a 2Å-long oxide layer. Each domain of HfO_2-based layer is assigned with a different set of α_i and β_i values for GLK model equation, as in (1), and the variations of α_i and β_i values follow a Gaussian distribution with median α and β values fitted to the experimental data of remnant polarization (P_r) and coercive field (E_c) for undoped and 5 mol% Al-doped HfO_2 thin films [6].

C. *TCAD Simulation for Fe-NAND Device with Al:HfO_2*

The characteristics of multi-domain ferroelectric behavior are simulated using TCAD [10] in a two-dimensional (2D) Fe-NAND device structure with cylindrical symmetry around the cylinder center to model three-dimensional (3D) effects. The device is composed of three cells with a wordline (WL) length and spacing of 20 and 30 nm, respectively, and a radius of filler oxide of 20 nm. The layer stack consists of 6 nm-thick Si as channel, and a combined gate dielectric of 13 nm-thick HfO_2-based ferroelectric layer and 1 nm-thick SiO_2 layer. The source line (SL) and bitline (BL) regions are of n-type with doping level of $1x10^{20}$ cm^{-3}. Fig. 2(a) and (b) illustrate the schematic and the layer stack of Fe-NAND device used in our simulations.

In the simulations, the HfO_2-based layer is divided into 81 regions with 5 nm-long grain size, separated by a 2Å-long oxide layer. Each HfO_2-based domain is assigned with a parameter set of Gaussian distributed α_i and β_i values with median values of GLK model calibrated from section II-A. To study the grain-to-grain variability, we further introduce the randomness while assigning parameters in each domain. Apart of polarization, the low-field mobility is modeled using the Lombardi model, while

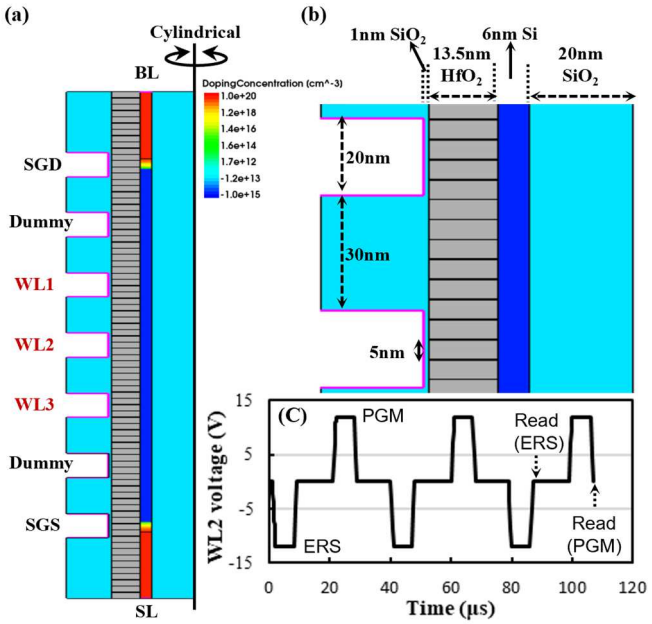

Fig. 2. (a) Schematic of Fe-NAND. (b) Layer stack of Fe-NAND. (c) Applied bias voltage evolution for erase/program cycle.

in high driving field, the mobility is modeled using the Canali model. Additionally, the carrier generation and recombination are considered through the Shockley–Read–Hall (SRH) model and the carrier tunneling is modeled using the nonlocal band-to-band tunneling model.

To characterize Fe-NAND properties, all the cells are first erased by a 6 µs-long pulse at -12V with SL and BL being grounded. Then, a pulse voltage of 12V is applied at the center selected WL cell (i.e., WL2) for programming while keeping other terminals grounded. The waiting time between erase (ERS) and program (PGM) operations is 10 µs. Fig. 2(c) presents the evolution of bias conditions for three ERS/PGM cycles at WL2. Toward the end of three ERS/PGM cycles, the read operation is performed by applying 8V to the pass (non-selected) cells, 0.5V to BL, and 0V to SL. The threshold voltage of the selected cell is determined at BL current of 5e-7 A by sweeping WL voltage.

III. Results

A. *Polarization Model Parameters Extraction from Atomic Simulation for Al:HfO_2 Bulk*

The orthorhombic phase allows for a finite polarization controlled by the oxygen position and the resulting change of

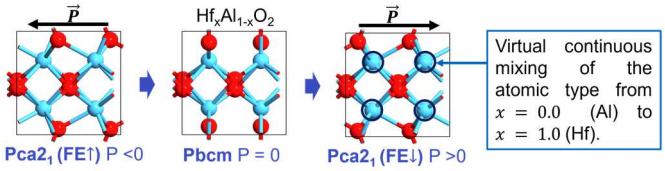

Al content (mol%)	0	5	10
Volume (Å^3)	132.3 (a=5.04Å)	141.9 (a=5.24Å)	143.4 (a=4.62Å)
P (µC/cm^2)	70.0	79.6	53.1

Fig. 3. Switching path of Al:HfO_2 with up/down/unpolarized configurations labeled by symmetry groups. Al mixing is simulated at 0, 5, and 10 mol%.

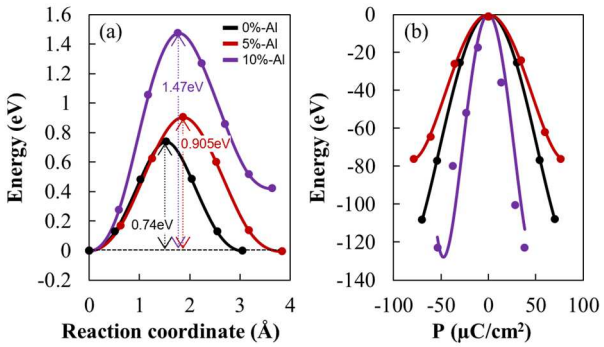

Fig. 4. (a) DFT NEB barrier calculation for various Al contents. (b) Energy-polarization curves from DFT with GLK models fitted parameters for undoped HfO_2, 5 mol% Al:HfO_2 and 10 mol% Al:HfO_2 (same labels as in figure (a)).

space group symmetry. Energetically the monoclinic phase is dominant in ideal bulk, while thin-film surfaces and defects make the orthorhombic phase energetically favorable. Our investigation in this paper is focused on the role of Al doping on the performance of polar orthorhombic HfO_2. Fig. 3 illustrates polarization switching mediated by oxygens displacement and polarization values for Al:HfO_2 bulk. A significant volume expansion with Al content is found, which is due to a larger atomic radius of Al compared to Hf. The polarization with 5 mol% Al is simulated to be 79.6 μC/cm^2, which is approximately 14% larger than the undoped case (70.0 μC/cm^2), while it decreases again at 10 mol% Al (53.1 μC/cm^2). The polarization switching relies on the movement of oxygen atoms along the shown transition path. At low Al content, the volume expansion is an isotropic strain effect. However, at 10 mol% Al, the expansion is anisotropic: the unit cell contracts in polarization direction (lattice vector a), while it expands in directions transverse to polarization. Hereby, the oxygens can move into a more symmetric alignment and it leads to a lower polarization.

Fig. 4(a) illustrates the full switching energetics obtained from NEB. The switching barrier increases by 22%, from 0.74 eV to 0.91 eV, with incorporation of 5% mol Al dopants. Meanwhile, the barrier increases to 1.47 eV at 10% mol Al content, which is approximately two times of the undoped case. Consequently, the coercive field needed for inducing the polarization switching increases significantly at 10% Al, while the polarization decreases relative to the undoped case. This comparison indicates that 5mol% Al:HfO_2 is a good

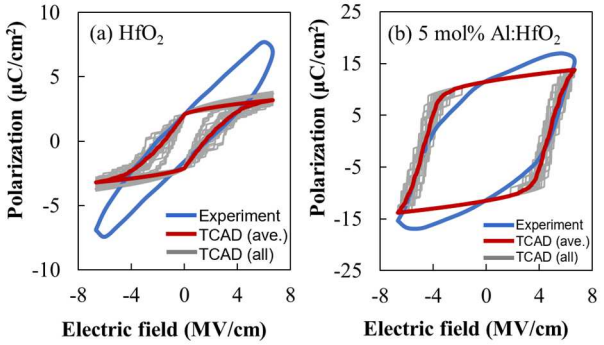

Fig. 5. P-E hysteresis of multi-domain GLK model with fitted parameters and experimental data for (a) undoped HfO_2 and (b) 5 mol% Al:HfO_2.

configuration for maintaining a low switching barrier while demonstrating a relatively large remnant polarization. It is noted that the calculated remnant polarization values for Al:HfO_2 bulk are generally larger than the experimental values reported in [6], which implies that the Al:HfO_2 thin films are not composed of ideal ferroelectric phase in all volume.

Furthermore, the polarization calculations and NEB transition barrier calculations were combined to obtain the energy-polarization analysis, which can be used to extract Landau coefficients in GLK model. Fig. 4(b) presents the resulting energy-polarization curves with the fitted GLK model parameters and 5mol% Al:HfO_2 is found to exhibit a larger value of polarization maximum at low energy barrier penalty, which is in agreement with experimental results [6]. This showcases a direct workflow for characterizing the ferroelectric performance of single grain in a specific atomic structure with Al doping. Meanwhile, the remnant polarization discrepancy between atomistic calculation and experiment data indicates the importance of nonpolar monoclinic grains, multi-domain dynamics, and defects, which can be further explored in the multi-domain model development.

B. Multi-Domain Polarization Model Parameter Calibration for Al:HfO_2 Thin Films

The HfO_2 with Al doping is known to improve ferroelectric characteristics by increasing the probability of triggering polar orthorhombic phase in the HfO_2 layer [6]. The experimental results of Chen *et al.* [6] show that the remnant polarization and the coercive field for 5 mol% Al-doped HfO_2 thin film are 11.5 μC/cm^2 and 4.6 MV/cm, respectively, which are higher than the undoped HfO_2 thin film (P_r = 2.1 μC/cm^2; E_c = 1.6 MV/cm). The GLK polarization model calibration on MFM capacitors described in section II-B are performed with respect to experimental results of Chen *et al.* The calibrated median values of Gaussian distributed parameters are listed in Table I for undoped and 5 mol% Al:HfO_2 thin films and the corresponding polarization-electric field (P-E) hysteresis loops simulated by TCAD are compared to experimental data and shown in Fig. 5.

TABLE I. CALIBRATED MEDIAN VALUES OF GAUSSIAN DISTRIBUTED PARAMETERS IN MULTI-DOMAIN GLK POLARIZATION MODEL

GLK parameter	α_i	β_i	γ	G
	cm/F	cm^5/(FC^2)	cm^9/(FC^4)	cm^3/F
HfO_2	-1.35E12	1.46E23	0	1E-3
5 mol% Al:HfO_2	-5.57E11	2.0E23	0	1E-3

C. Characteristics of Fe-NAND with Al:HfO_2

The multi-domain GLK polarization model with Gaussian distributed parameters, whose median values are from Table I, is implemented in a Fe-NAND device and Fig. 6 shows the 2D polarization plots after ERS and PGM operations. It can be observed that the Fe-NAND with 5 mol% Al:HfO_2 has a stronger remnant polarization in the ferroelectric layer than the

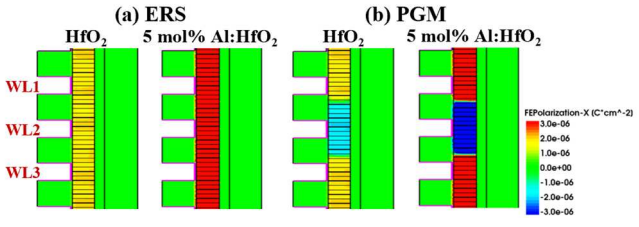

Fig. 6. Polarization plots for Fe-NAND with undoped HfO_2 and 5 mol% Al:HfO_2 thin films in (a) erase state for all WLs and (b) program state for WL2.

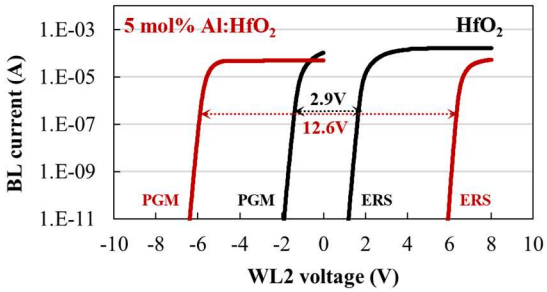

Fig. 7. IdVg curves for selected cell in ERS and PGM states.

one with HfO_2, which is consistent with the MFM capacitor results shown in Fig. 5.

In Fig. 7, the drain current-gate voltage curves are presented for ERS and PGM states. The MW determined as the threshold voltage (Vt) differential between PGM and ERS states. For the Fe-NAND with undoped HfO_2 layer, MW is extracted to be 2.9V. While for the Fe-NAND with 5 mol% Al:HfO_2 layer, it shows a superior MW reaching 12.6V, which is beneficial for the realization of QLC operation. Moreover, the threshold voltage variations due to grain-to-grain grain variability are examined as well for selected cell and unselected neighbor cell. As shown in Fig. 8(a) and 8(b), the 3-sigma standard deviations (3σ-SD) of Vt changes for the selected cell with 5 mol% Al:HfO_2 are about 0.57 V and 0.63 V, respectively, in PGM and ERS states. As for the unselected neighbor cell, the Vt changes attributed to the PGM disturbance from selected cell are slightly larger with the 5 mol% Al:HfO_2 case and it can be further reduced with proper WL spacing.

IV. Conclusions

The ferroelectric effect and variability of HfO_2-based thin films are related to the ratio and the distribution of ferroelectric orthorhombic phase, which are dependent on the process conditions and the element doping. Here, we perform atomistic simulations to examine the ferroelectricity with Al doping in HfO_2 bulk and demonstrate a polarization enhancement at 5 mol% Al content due to the unit cell volume expansion. This ferroelectric behavior is also observed experimentally in Al:HfO_2 thin films. To proceed with Fe-NAND characteristics simulations, a multi-domain GLK polarization model is implemented with parameters being calibrated from the measured P-E hysteresis. Based on it, the PGM and ERS states of Fe-NAND are simulated for Al:HfO_2 material and a large MW of 12.6V is obtained with Al dopant incorporation and the 3σ-SD of Vt change in PGM state due to the grain-to-grain variability is estimated to be 0.57 V. The enhanced ferroelectric

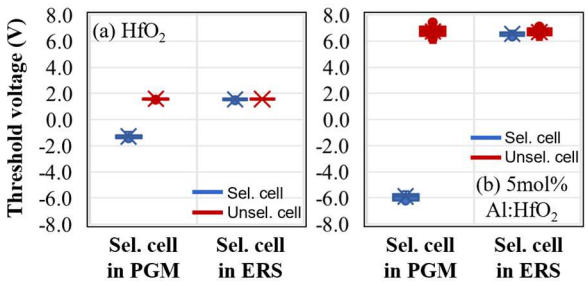

Fig. 8. Vt variations of selected cell and unselected neighbor cell for (a) HfO_2 and (b) 5 mol% Al:HfO_2 thin films when selected cell is in PGM or ERS state.

characteristic comes from the increased probability of orthorhombic phase with Al doping and the variability can be improved through process optimization.

Acknowledgment

The authors would like to thank Pawel Lenarczyk and Pavel Tikhomirov for the fruitful discussion.

References

[1] C. L. Jia, S. B. Mi, K, Urban, I. Vrejoiu, M. Alexe, and D. Hesse, "Atomic-scale study of electric dipoles near charged and uncharged domain walls in ferroelectric films," Nature materials, vol. 7, pp. 57 (2008).

[2] S. Yoon, S. Hong, D. Kim, G. Choi, Y. M. Kim, K. Min, S. Kim, M. Na, S. Cha, "QLC programmable 3D ferroelectric NAND flash memory by memory window expansion using cell stack engineering," *2023 Symposium on VLSI Technology and Circuits (VLSI Technology and Circuits)*, Kyoto, Japan, 2023, pp. 1-2.

[3] D. Das, H. Park, Z. Wang, C. Zhang, P. V. Ravindran, C. Park, N. Afroze, P. K. Hsu, M. Tian, H. Chen, W. Chern, S. Lim, K. Kim, K. Kim, W. Kim, D. Ha, S. Yu, S. Datta, A. Khan, "Experimental demonstration and modeling of a ferroelectric gate stack with a tunnel dielectric insert for NAND applications," 2023 IEEE International Electron Devices Meeting (IEDM), San Francisco, CA, USA, 2023.

[4] K. Florent, S. Lavizzari, L. Di Piazza, M. Popovici, E. Vecchio, G. Potoms, G. Groeseneken, and J. Van Houdt, "First demonstratation of vertically stacked ferroelectric Al doped HfO_2 devices for NAND applications," *2017 Symposium on VLSI Technology*, Kyoto, Japan, 2017, pp. T158-T159.

[5] K. Florent, M. Pesic, A. Subirats, K. Banerjee, S. Lavizzari, A. Arreghini, L. Di Piazza, G. Potoms, F. Sebaai, S. Mcmitchell, M. Popovici, G. Groeseneken, and J. Van Houdt, "Vertical ferroelectric HfO_2 FET based on 3-D NAND architecture: towards dense low-power memory," 2018 IEEE International Electron Devices Meeting (IEDM), San Francisco, CA, USA, 2018, pp. 2.5.1-2.5.4.

[6] S. Chen, P. Qin, J. Yang, M. Chen, Q. Du, Y. Kong, Y. Liu, and D. Cao, "Ferroelectricity in the Al doped HfO_2," J. Alloys and Compounds, vol. 965, pp. 171456, November 2023.

[7] J. Y. Park, D. H. Choe, D. H. Lee, G. T. Yu, K. Yang, S. H. Kim, G. H. Park, S. G. Nam, H. J. Lee, S. Jo, B. J. Kuh, D. Ha, Y. Kim, J. Heo, and M. H. Park, "Revival of ferroelectric memories based on emerging fluorite-structured ferroelectrics," Advanced Materials, vol. 35, pp. 2204904 (2023).

[8] B. Ku, S. Choi. Y. Song. And C. Choi, "Fast thermal quenching on the ferroelectric A;:HfO_2 thin film with record polarization density and flash memory application," 2020 IEEE Symposium on VLSI Technology, Piscataway, NJ, USA, 2020, pp. 1-2.

[9] S. Smidstrup *et al.*, "QuantumATK: an integrated platform of electronic and atomic-scale modelling tools "J. Phys. Condens. Matter. 32, 015901 (2020).

[10] Sentaurus Device User Guide, Synopsys, CA, USA, Sep. 2 (2023).